Multi-omics characterization of human kidneys identifies cPLA2-arachidonic acid metabolism as a potential driver of inflammation

Evans Asowata
AstraZeneca
Simone Romoli
AstraZeneca
Jennifer Tan
AstraZeneca
Scott Hoffmann
AstraZeneca
Margaret Huang
University of Cambridge https://orcid.org/0000-0001-5277-863X
Fynn Krause
University of Cambridge https://orcid.org/0000-0001-6664-2637
Benjamin Jenkins
University of Cambridge https://orcid.org/0000-0003-0038-9709
Daniel Jachimowicz
AstraZeneca
Rasmus Agren
AstraZeneca
Barbara Musial
AstraZeneca
Krishna Mahbubani
University of Cambridge https://orcid.org/0000-0002-1327-2334
Michael Murphy
University of Cambridge
Julian Griffin
Imperial College London https://orcid.org/0000-0003-1336-7744
Albert Koulman
University of Cambridge https://orcid.org/0000-0001-9998-051X
Pernille Hansen
AstraZeneca https://orcid.org/0000-0002-8202-3497
Stephanie Ling

AstraZeneca https://orcid.org/0000-0002-1237-091X

Kourosh Saeb-Parsy

University of Cambridge https://orcid.org/0000-0002-0633-3696

Kevin Woollard (kevin.woollard@astrazeneca.com)

AstraZeneca

Article

Keywords:

Posted Date: April 7th, 2022

DOI: https://doi.org/10.21203/rs.3.rs-1461691/v1

Abstract

The limited availability of human kidney biopsies to study acute kidney injury (AKI) has restricted the development of effective therapies for this condition. Here, we validate the use of deceased transplant organ donor kidneys to study human AKI and characterized the multi-omics and immune landscape of human AKI kidneys. We demonstrate that changes in kidney injury and inflammatory markers following AKI in deceased transplant donors are similar to that of mouse kidney ischemia-reperfusion injury. Integrated transcriptomic and metabolomic analysis of human kidneys shows upregulated renal arachidonic acid metabolism following AKI, a pathway speculated to be linked to the ceramide accumulation detected in these kidneys. Markers of T and B lymphocytes, and macrophages were upregulated in AKI kidneys. Interestingly, we show upregulated renal cytoplasmic phospholipase A2 (cPLA2) levels in AKI kidneys, and the inhibition of this enzyme reduced injury and inflammation in vitro, findings that have potentially important therapeutic implications.

Introduction

AKI is a sudden decline in kidney function, which is currently diagnosed by an abrupt increase in serum creatinine and/or a significant decrease in urine output, and is associated with significant healthcare cost and mortality [1-3]. There is currently no effective pharmacological therapy for AKI and the current treatment involves the management of AKI symptoms using renal replacement therapies and hemodynamics optimization [1,4]. Translational barriers from rodent models of AKI to patients in clinic are among the major contributors to the lack of effective treatment strategies for AKI [5,6]. The considerable degree of heterogeneity in clinical manifestation of AKI, age, existing comorbidities (e.g. diabetes and cardiovascular disease) and drug exposures of patients are key risk factors that may influence the treatment outcomes of AKI patients [6]. These factors are almost never replicated in pre-clinical experiments and as a result, potential AKI treatment strategies developed from pre-clinical data have failed to demonstrate clinical benefits. In addition, the mouse and human immune system have been shown to exhibit key differences [7], and the immune cell population of the kidneys obtained from these species has been reported to have different proportions of innate and adaptive immune cells [8]. Since kidney inflammation is a key driver of AKI [9], the differences in the composition of immune cells in these species and the potential differences in the immune response to AKI may contribute to the translational barriers in AKI research. Because kidney biopsies are very rarely performed in AKI patients, investigating the renal immune cell landscape and structural changes in the human kidney following AKI is inherently challenging and thus, there is limited human data regarding the immunoregulatory mechanisms underlying AKI.

Although lipids are the main source of energy for physiological processes in the kidney, abnormal lipid metabolism has been demonstrated to mediate renal inflammation, epithelial cell death and fibrosis [10-13]. There is evidence that the critical early events that determine the progression and outcome of AKI develop from damage to the phospholipid-enriched plasma membrane of cells and associated sub-cellular

membranes, and the subsequent activation of phospholipases within the kidney [14]. Specifically, accumulating evidence in pre-clinical models suggest that cPLA2 drives the progression of various forms of kidney disease [15-18]. Abnormal renal phospholipid metabolism by cPLA2 leads to the generation of arachidonic acid from which bioactive metabolites (e.g. prostaglandins and leukotrienes) that promote cellular inflammatory cascade are generated [19]. Prostaglandin E2 (PGE2), generated via the cyclooxygenase pathway, has been shown to mediate diabetic nephropathy [20,21] and inflammation following ischemic AKI in preclinical models [22]. In addition, leukotrienes promote the accumulation and activation of immune cells in response to tissue injury and inflammation [23]. Whether the renal phospholipid-cPLA2-arachidonic acid pathway significantly contributes to the progression of AKI in humans or whether the reported changes in this pathway following AKI in pre-clinical models [19,24,25] translate to humans remains to be seen.

Despite the recent advances in understanding the important roles of lipids, metabolites and related enzymes in mediating kidney disorders [26-28] and the well characterised single-cell transcriptomic landscape of human kidneys [29,30], there is limited integrated multi-omics data identifying and validating potential metabolic pathways driving human AKI. Moreover, based on the important role of the immune system in mediating kidney damage, understanding the changes in the immune cell population and the metabolic pathways that are significantly impacted following AKI will be essential to unravel the mechanisms underlying lipid or metabolite-induced kidney inflammation in humans. The current study utilizes human kidneys donated by deceased transplant organ donors to study the multi-omics and immune cell landscape of human kidneys following AKI. Because the use of deceased donor kidneys as a model of human AKI has not been previously reported, we aimed to validate this model by comparing the changes in the levels of kidney injury and inflammatory markers, and histological changes in human kidneys with our findings in a commonly used mouse model of AKI induced by bilateral ischemia-reperfusion (IR) kidney. Deceased donor kidneys and renal proximal tubular epithelial cells (RPTECs) were then used to identify and validate the phospholipid-cPLA2-arachidonic acid metabolic pathway as a potential driver of kidney injury and inflammation following AKI in humans.

Methods

Deceased transplant kidney collection and donor characteristics

Informed consent was obtained from donor families for the use of the human tissue for this study. This study was conducted in accordance with the guidelines contained in the Ethical approval obtained from NHS Health Research Authority, North East 2 Research Ethics Committee (REC Reference 15/NE/0408). Kidneys were collected from deceased transplant donors with or without pre-donation AKI, aged 42-81 years, (Supplementary Table 1 and 2). AKI was diagnosed in these donors based on the eGFR data obtained from donors' clinical information on the NHS database in accordance with the ethical guidelines, and the average duration (in days) between AKI diagnosis and organ donation was approximately 3 days. Following retrieval from donors, kidneys were preserved using ViaSpan or Soltran,

placed in cold storage on ice and shipped to Addenbrooke's hospital (Fig. 1a). Tissue for RNA extraction, tissue lysate preparation and multi-omics experiments were immediately frozen in liquid nitrogen and stored at - 80°C until the time of use.

Animal experiment

Male mice (C57BL/6J), aged 6-8 weeks and weighing 18-22g, were purchased from Charles River Laboratories, UK. Mice were housed in pathogen-free facilities, maintained on a 12 hour light/dark cycle with ad libitum access to food and water. Mice from the same litter were randomly picked to undergo sham-operation or ischemia-reperfusion injury (IRI) to induce AKI. Mice were anaesthetized using 1.5–2% isoflurane and 2.0 L/min oxygen, and their core temperature maintained at ~ 37.0 °C throughout the duration of the experiment using a heat mat. Midline laparotomy was performed to access the left and right renal hila and ischemia was induced in both kidneys for 25 mins using a Micro-Serrofine clamp (15 mm, Fine Science Tools, Germany). Following ischemia, the Micro-Serrefine clamps were removed from the renal hila to restore blood circulation to both kidneys. The midline laparotomy was closed in two layers using 5-0 absorbable suture (Safil®, Braun, Germany) and mice were re-hydrated with 500 µL saline injected intraperitoneally. For the sham-operation, this procedure was repeated without clamping the left and right renal hila. Mice were allowed to recover for 24 hours following which blood and kidney tissue were collected. All procedures were approved by the UK Home Office under the Animal (Scientific Procedures) Act 1986.

Serum biochemistry

Blood samples collected from donors just before organ retrieval were kept at room temperature to clot after which the blood clot was removed, and the blood was spun at 2000 g for 10 minutes to obtain serum. Blood samples were also collected from mice 24 hours following IRI or sham-operation to obtain serum. Human and mouse serum samples were sent to core biochemical assay laboratory (CBAL) at Addenbrooke's hospital for the measurement of creatinine, BUN and levels of inflammatory cytokines, IL-1β, IL-6, IL-8 (mKC for mouse), IL-10, IL-18 (human only), IFN-γ (mouse only) and TNF-α.

Mass spectrometry imaging

Snap frozen kidney samples were embedded into a hydrogel of 7.5% HPMC/2.5% PVP as previously described [31] and cryosectioned using a CM1950 cryostat (Leica, Nussloch, Germany) to 10 µm thickness. Sections were thaw-mounted onto Superfrost glass slides and dried using the vacuum suction of the instrument to suck air across the tissue to minimize formation of aerosols, before vacuum packing in a slide mailer and storage at −80 °C [32]. Prior to mass spectrometry imaging (MSI), slides were thawed to room temperature before being unpacked to avoid analyte delocalisation through moisture condensation on the chilled slide surface. Before acquisition, slides were UVC-decontaminated as previously described to limit aerosolization and exposure to pathogens [33], with a refined approach using an exposure controlled system that irradiated the samples with 250mJ/cm^2 to limit analyte degradation.

Desorption electrospray ionisation (DESI)-MSI was performed on an automated 2D DESI stage (Prosolia Inc., Indianapolis, IN, USA) equipped with a custom-built sprayer assembly [34] mounted to a Q-Exactive Plus instrument (Thermo Scientific, Bremen, Germany). Analysis was performed in positive on one section and negative ion mode on the sequential section in full scan mode between m/z 70 and 1000 with 75µm spatial resolution, SLens setting of 75, capillary temperature of 320 °C, and a mass resolution of 70 000 at m/z 200 in profile ion mode. Automatic gain control was turned off. Electrospray solvent was methanol/water (95:5 v/v) at a flow rate of 1.5 µL/min, a spray voltage of ±4.5 kV, and nebulizing gas pressure of 6.5 bar (Nitrogen N4.8, BOC). Solvent was supplied using an Ultimate 3000 standalone nanoLC pump (Thermo Scientific Dionex, Sunnyvale, CA, USA). The DESI-MSI raw files were converted into mzML files using ProteoWizard msConvert [35] (v.3.0.4043), subsequently compiled to imzML files (imzML converter [36] v.1.3), and uploaded into SCiLS™ Lab MVS Premium 3D version 2021a (Bruker Daltonics, Bremen, Germany) for analysis and generation of a list of root mean square normalised mean peak intensity for each tissue.

Significantly modulated m/z peaks between AKI and control kidney cortex were calculated using two-tailed Mann Whitney *U* test, followed by Benjamini Hochberg multiple testing correction. Metabolites with adjusted p-value < 0.05 were considered as significantly differentially modulated in AKI kidney cortex compared to control. Pathway enrichment analysis was performed using MetaboAnalyst 5.0 [37] within tolerance of 5 ppm, with m/z peaks mapped to metabolites using KEGG annotations [38]. Adducts used in DESI positive mode include M+H [1+], M+Na [1+], M+K [1+]; adducts used in DESI negative mode include M-H [1-], M-H2O-H [1-], M-H+O [1-], M-Cl [1-].

Total RNA sequencing

Frozen kidney cortex tissue were put in RNA*later* stabilization solution (Thermo Fisher Scientific, UK) and stored at -80°C until use. Samples were moved into Agencourt RNAdvance Tissue kit (Beckman Coulter) lysis buffer and homogenized at 1000 rpm for 2min with 5mm Stainless Steel Bead (Qiagen) using 1600 MiniG Tissue Homogenizer (SPEX SamplePrep). Next, total RNA was extracted using Agencourt RNAdvance Tissue kit including DNase treatment for 15min at 37˚C (Ambion DNaseI, ThermoFisher) on an automated Biomek i7 Hybrid system (Beckman Coulter). RNA quantification and quality control was performed on 48 capillary Fragment Analyzer 5300 system (Agilent). All samples showed fragment distribution values (% DV200) above 74 and were subjected to a total RNA-seq library preparation using KAPA RNA HyperPrep Kit with RiboErase (Roche) with 450ng of input RNA, 5min fragmentation at 95 ˚C, and 9 PCR cycles performed on a Tecan Fluent 1080 system (Tecan). Resulting libraries were quantified on 48 capillary Fragment Analyzer 5300 system showing 295bp average peak size, and pooled equimolarly to a final concentration of 1.9nM. 51bp paired-end sequencing was performed on a v1.5 S1 NovaSeq6000 kit (Illumina) including 1% of 1.9nM PhiX v3 control (Illumina). Read quality for all libraries was accessed using FastQC (v0.11.7) (https://www.bioinformatics.babraham.ac.uk/projects/fastqc/), Qualimap (v2.2.2c) [39] and samtools stats (v1.9). Quality control (QC) metrics for Qualimap were based on a STAR (v2.7.2b) [40] alignment against the human genome (GRCh38, Ensembl v100). Next, QC metrics

were summarized using MultiQC (v1.9) [41]. Sequencing adapters were then trimmed from the remaining libraries using NGmerge (v0.3) [42]. A human transcriptome index consisting of cDNA and ncRNA entries from Ensembl (v100) was generated and reads were mapped to the index using Salmon (v1.1.0) [43]. Differential gene expression analysis (between control and AKI kidney cortex) was performed using edgeR (v3.36), with sex and fraction mitochondrial RNA as covariates.

Gene set enrichment analysis

Kyoto Encyclopedia of Genes and Genomes (KEGG) [38] and Gene Ontology (GO) [44] Gene Set Enrichment Analysis (GSEA) was performed using ClusterProfiler (version 4.0.5) [45]. Data is presented as ridgeplots showing the top 30 significantly enriched (FDR<0.05) gene sets, ranked by their absolute fold enrichment.

Integrated metabolomic and transcriptomic pathway analysis

Integrated metabolomic and transcriptomic pathway analysis was performed using the joint-pathway analysis function within MetaboAnalyst 5.0 [37] to identify pathways enriched based on altered gene expression levels and metabolite levels. Up-regulated and down-regulated metabolites in kidney cortex from AKI donors compared to control were analyzed separately to generate pathways that are significantly ($p<0.05$) enriched. KEGG pathway map depicting fold changes in gene expression and metabolite levels between AKI and control kidney cortex was generated using Pathview [46].

Lipidomics

Lipids were extracted and analyzed using the protein precipitation liquid extraction protocol and liquid chromatography-mass spectrometry (LC-MS) method described previously [47]. For free fatty acid analysis, the remaining samples (~90 µL) following the lipid analysis was dried down and reconstituted in 90 µL of a solution containing methanol and water (3:1) with 0.1% acetic acid. Analysis of the free fatty acids was achieved using Waters Acquity H-Class HPLC System with the injection of 10 µL onto a Waters Premier CSH C18 column; 1.7 µM, I.D. 2.1 mm X 50 mm, maintained at 40 degrees Celsius. Mobile phase A was water with 0.1% acetic acid. Mobile phase B was methanol with 0.1% acetic acid. The flow was maintained at 500 µL/min through the following gradient: 0.00 minutes_75% mobile phase B; 5.00 minutes_99% mobile phase B; 7.00 minutes_99% mobile phase B; 7.50 minutes_75% mobile phase B; 10 minutes_75% mobile phase B. The mass spectrometer used was the Thermo Scientific Exactive Orbitrap with a heated electrospray ionisation source optimised for free fatty acid ionisation at a scan rate of 2 *Hz* (resolution of 50,000 at 200 *m/z*) with a full-scan range of *m/z* 70 to 500 in negative mode.

Both sets of data was quantified using the instrument proprietary software (Thermo Xcalibur) to calculate the area ratios of the intensity of the target analyte to the intensity of an appropriate internal standard, these area ratios were then converted into a semi-quantitative concentration by multiplying the area ratio by the concentration of that internal standard. The data was then quality checked, blank corrected and normalised to sample amount. Analysis of the concentration of lipids and free fatty acids between AKI

and control kidneys was carried out using the one-factor statistical analysis functionality within MetaboAnalyst (version 5.0) [37]. Raw data from lipid and fatty acid analysis was uploaded into the MetaboAnalyst analysis platform online, and heatmap, sparse partial-least square discriminant analysis (sPLS-DA), and volcano plot analysis were selected under the the one-factor statistical analysis functionality.

Kidney histology

Human and mouse kidneys for histology were fixed using 10% formalin overnight and then stored in 70 % ethanol at 4°C until paraffin embedding. The tissue was then processed using Leica TP1020 tissue processor (Leica Biosystems, IL, USA) and embedded in paraffin. Thin sections (4 µm thick) were cut using a microtome and mounted on a microscopic glass slide. Deparaffinized kidney sections were rehydrated and stained with Periodic Acid Schiff (PAS) reagents (ThermoFischer Scientific, UK) according to manufacturer's protocols.

Imaging mass cytometry

IMC immunostaining was carried out as previously described [48].Two FFPE sections, one section was first stained with H&E to identify a region of interest that would then be stained using our validated IMC metal-conjugated antibody panel (**Supplementary Table 4**). Deparaffinization of tissues and subsequent antigen retrieval was performed using the Leica Bond (Leica Bond RX, Leica Biosystems) automated system. The antigen retrieval method used heat induced epitope retrieval (HIER) and an EDTA (pH=9) based retrieval buffer. Following antigen retrieval, tissues were washed in PBS and blocked using a casein solution for 30 min. An antibody cocktail containing all the antibodies in the panel were applied and incubated overnight at 4 °C. Readily available metal conjugated antibodies were acquired directly from Fluidigm®. Custom antibodies were conjugated using the MaxPar® antibody conjugation kit, according to manufacturer's guidelines. Following incubation, slides were washed 3 times, 5 mins each, in PBS and a DNA intercalator was applied for 30 mins at room temperature. The slide was then washed 3 times, 5 mins each, in PBS and a final wash in distilled water for 1 min before drying the slides at room temperature. IMC analysis was performed using the Hyperion Imaging System (Fluidigm Corporation, San Francisco, CA, USA). Laser tissue ablation was performed at a laser power of 4 db, tuned to fully ablate the tissue without etching the glass slides, at a frequency of 200 Hz. Imaged areas were 1.8x1.8 mm.

Imaging data was exported as 32-bit ome.tiff using MCDViewer and imported into Halo (Halo®, Indica Labs) for subsequent cell segmentation and thresholding. The DNA intercalator at 191 and 193 Ir was used to detect nuclei and cell segmentation was performed using the HighPlex FL v3.1.0 module. The proportion of cells expressing the different markers in the kidney cortex (glomerular and tubule-interstitial component) were compared between AKI and control samples. The stained section was further sub-classified into glomerular and tubulo-interstitial regions using a DenseNet classifier in order to identify the relative proportion of cells expressing specific markers in specific regions of the kidney. Thresholding was manually set for each individual channel.

Quantitative real-time polymerase chain reaction (qRT-PCR)

Total RNA was isolated from human kidney cortical slices and whole mouse kidney using TRIzol™ reagent according to manufacturer's instructions (Life Technologies, Paisley, UK) and quantified using NanoDrop™ spectrophotometer. Using human and mouse specific primers (**Supplementary Table 5**), qRT-PCR was carried out to detect the mRNA expression levels of KIM-1, NGAL, and enzymes involved in fatty acid metabolism: cPLA2, CPT1A, CPT2, ACOX1, ACOX2, PPARA, PPARGC1A, CD36 (human only). All primers were purchased from Life Technologies, Paisley, UK. For PCR reaction, cDNA synthesized from 1µg of RNA was diluted (1:10) and the diluted cDNA (0.5µl) was added to primer for the gene of interest (0.1µl), house-keeping gene (0.1µl), TaqMan master mix (1.0µl) and nuclease-free water (0.3µl) to prepare the reaction mix. HPRT1 was used as the house-keeping gene for all PCR reactions. qRT-PCR experiment was performed using QuantStudio 12K Flex Real-Time PCR System (Life Technologies, Paisley, UK) with the following reaction conditions: 50°C for two minutes, 95°C for two minutes, 40 cycles of 95°C for 1 second followed by 60°C for 20 seconds. Relative quantification of the gene expression of the markers of interest were normalised using the expression of an endogenous control, HPRT1 (VIC ^{TM} probe, ThermoFisher Scientific, UK), and expression levels determined using the $2^{-\Delta CT}$ formula.

Kidney tissue lysate preparation

Human cortical slices and whole mouse kidney were homogenized in MSD Tris lysis buffer (R60TX-3) containing protease and phosphatase inhibitors (R70AA-1). Tissue was homogenized for 2 minutes using a hand-operated homogenizer set at the highest speed. Homogenized samples were centrifuged at 8000 rpm for 10 minutes and the supernatant was collected. Protein concentration of the supernatant samples was determined using Pierce^{TM} BCA Protein Assay Kit (Thermo Fisher Scientific, UK). Samples were stored at -80°C until use.

Kidney cytokine assay

Human kidney tissue lysate samples were analyzed for the levels of IL-1β, IL-6, IL-8 and TNF-α using the V-PLEX proinflammatory panel 1 human kit (K15049D-1) and the levels of CCL2 were investigated using the U-PLEX human MCP-1 assay kit (K151UGK). Mouse kidney tissue lysate were analyzed using the mouse proinflammatory 7-plex kit (K15012B-1) for the levels of IL-1β, IL-6 and mouse keratinocyte-derived chemokine (mKC), which is homologous to human IL-8. All assays were carried out following manufacturer's instructions.

Western blotting

Western blotting experiment was carried out following previously described protocol [49]. Kidney tissue lysate were mixed with laemmli buffer and separated using 4-20% mini-PROTEAN precast gel. Protein were then transferred on to a PVDF membrane by electroblotting. PVDF membrane containing the protein of interest was incubated in PBS-tween containing CPT1A (ab128568) or cPLA2 (ab58375) antibody overnight at 4°C. Following incubation, the primary antibody was washed off and the membrane

incubated using the appropriate secondary antibodies. The bands for each protein of interest were detected using ECL and the intensity of each band was quantified using image J. Following the detection of CPT1A or cPLA2, the antibodies were stripped off and the membrane incubated with GAPDH (ab8245) and the appropriate secondary antibody and the bands detected as described above. The protein levels of CPT1A and PLA2 relative to GAPDH were represented in arbitrary unit (a.u).

Primary cell culture

Renal proximal tubular epithelial cells (RPTEC) were obtained from Lonza Bioscience (Cat #. CC-2553) and cultured in fully supplemented REGM^{TM} cell culture medium (Cat #. CC-3190) until they are 70% confluent. Cells were detached using Accutase ^{TM} and approximately 30,000 cells were plated in a 24 well plate in fully supplemented medium for 24-48 hours until 100% confluent. Cells were either incubated with supplement free medium (vehicle) or treated with 100 ng/ml IL-1β, with or without a cPLA2 inhibitor (a kind gift from Medicinal Chemistry, AstraZeneca), at 10 or 100 μM, for 6 hours as illustrated in Fig. 5a. Cell culture medium was collected from each well and analyzed for the levels of PGE2, KIM-1, IL-6, IL-8 and TNF-α.

Kidney organ culture

Human kidney organ culture were carried out as previously described [50,51]. Approximately equal amount of kidney tissue fragments (each ~ 1 mm^3) were dissected from 4 human kidneys collected from 3 female donors (Fig. 5g) and cultured for 12 hours in Essential 6^{TM} (E6) medium (Cat #. A1516401). Tissue fragments were either incubated with medium only (vehicle) or treated with 200 ng/ml IL-1β, with or without 100 μM cPLA2 inhibitor. The change in the levels of PGE2 and KIM-1 released into the culture medium following a 12-hour incubation period were compared between IL-1β -and IL-1β + cPLA2 inhibitor-treated tissue.

Statistical Analysis

Data from deceased transplant donor characteristics is presented as mean ± standard deviation (SD) and all other data is presented as mean ± standard error of mean (SEM). Unless otherwise stated, statistical analysis was performed using GraphPad Prism 9.0 software. Mann Whitney *U* test was used to compare data from donors with AKI versus control donors, Pearson correlation was used to compute the coefficient of correlation (r) values and volcano plot was generated to visualize significant fold change of genes of interest. Statistical significance was depicted as *$P < 0.05$, **$P < 0.01$, ***$P < 0.001$ or ****$P < 0.0001$.

Results

Validation of deceased transplant kidney donors as a model of human AKI

We collected human kidneys that were donated for transplantation, but were subsequently declined due to reasons unrelated to physiological function (Table 1 and Supplementary Table 1). Kidney and blood samples collected from donors at the point of organ donation were placed in cold storage and sent to the laboratory for experiment as illustrated in Fig. 1a. A total of 22 kidneys were collected from 15 deceased organ donors with historically normal kidney function, who developed AKI (donors with an increase in serum creatinine ≥ 26.5μmol/l or 0.3mg/dl [52] or a decrease in eGFR of > 20ml/min/1/73m^2 over a 48 hour window) and donors that did not develop AKI (control) during the last few days preceding to organ donation (Supplementary Table 1). The likely cause of AKI in the donors may have been due to cardiac arrest, infection or sepsis during hospital admission following intercranial hemorrhage (in 11 donors), hypoxic brain damage (in 3 donors) or myocardial infarction (in 1 donor) (Supplementary Table 1). The donors in the AKI and the control group were matched for age, sex, body mass index and the cold ischemic time (CIT) of the kidneys before sample collection (Table 1). As expected, terminal serum creatinine was significantly higher in donors with AKI compared to control donors (Fig. 1b), while BUN levels were unchanged (Fig. 1c). Serum interleukin 6 (IL-6) and tumor necrosis factor-alpha (TNF-α) levels were significantly higher in donors with AKI (Fig. 1d), suggesting systemic inflammation in this group of donors. Quantitative PCR experiment on kidney tissue showed a significant upregulation of kidney injury molecule 1 (KIM-1) (Fig. 1e) and neutrophil gelatinase-associated lipocalin (NGAL) mRNA (Fig. 1f). ELISA using kidney tissue lysate showed a significant upregulation of KIM-1 protein in kidneys of donors with AKI compared to control donors (Fig. 1g), while NGAL protein levels were unchanged (Fig. 1h). Periodic Acid Schiff (PAS) staining (Fig. i) showed significant tubular injury in the kidneys of donors with AKI (Fig. j), characterized by tubular casts, loss of brush border membrane and vacuolated tubules, indicated by arrows (Fig. i). The levels of renal inflammatory markers interleukin 1 beta (IL-1β) (Fig 1k), IL-6 (Fig. 1l) and C-C motif chemokine ligand 2 (CCL2) (Fig. 1n) were significantly higher, with a trend for higher levels of interleukin 8 (IL-8) in kidney lysates of donors with AKI compared to control donors (Fig. 1m).

In mice, IR kidney injury resulted in significantly higher levels of serum creatinine, BUN, IL-10 and TNF-α (Supplementary Fig. 1a, b, f, g) suggesting that the significant decline in kidney function following AKI is associated with systemic inflammation as seen in the human kidney donors. In addition, the mRNA expression of renal KIM-1 and NGAL, the protein levels of IL-1β, IL-6 and KC, and the degree of tubular damage were significantly higher in the kidney of mice following IR injury compared to sham-operated animals (Supplementary Fig. 1i -o). In summary, changes in the levels of kidney injury and inflammatory markers, and tubular injury in kidneys following AKI in our mouse kidney IR injury and deceased human kidney models are consistent with data from pre-clinical cellular models of AKI and studies using human kidney biopsies patients [53-55]. These findings validate the use of deceased transplant organ donor kidneys as a reliable model to study human AKI.

Multi-omics analysis of deceased transplant kidney donor model of AKI

Untargeted mass spectrometry-based metabolomic profiling of human kidney cortex from all donors was carried out to identify metabolites that are differentially expressed in kidneys from AKI donors compared to control donors. Peaks were detected for a total of 8978 m/z values in our human kidney cortex

samples (5010 in positive and 2968 in negative mode). In order to putatively identify the metabolites that correspond to the peaks detected at different m/z values, we mapped the m/z values against the metabolites in the KEGG metabolite database [38] with a m/z tolerance of 5 ppm. A total of 484 metabolites were putatively identified and the differential abundance of these metabolites in the kidney cortex of AKI donors compared to controls is shown in Supplementary Table 6. Using pathway enrichment analysis, we showed that arachidonic acid metabolism, linoleic acid metabolism and six other metabolic pathways were significantly upregulated, while steroid biosynthesis was downregulated in kidney cortex of AKI donors compared to controls (Fig. 2a). Next, we performed total RNA sequencing to investigate differentially expressed genes in the kidney following AKI. Expression of a total of 21,628 genes were detected in our human kidney cortex samples and the differential expression of the detected genes in AKI kidney cortex compared to control is shown in Supplementary Table 7. The metabolomic and transcriptomic data were integrated using the joint pathway analysis function within MetaboAnalyst 5.0 [37] to identify metabolic pathways enriched based on altered gene expression levels and metabolite levels. Among the significantly upregulated pathways, arachidonic acid metabolism was identified as the pathway with the highest fold enrichment (Fig. 2b). In addition, increased gene expression of NAD-dependent oxidoreductases (KEGG Entry: EC 1.1.1.21) (Supplementary Fig 2a-c) and ATP-dependent hexokinases (KEGG Entry: EC 2.7.1.1) (Supplementary Fig 2a & c) were associated with pentose and glucuronate interconversion, fructose and mannose, and galactose metabolism, which were among the top 6 pathways with the highest fold enrichment (Fig. 2b). Volcano plot analysis of the differentially expressed genes in the arachidonic acid pathway as highlighted in the KEGG online database (Entry: hsa00590) showed that arachidonate 5-lipoxygenase (ALOX5) had the greatest fold change in the kidney cortex of donors with AKI compared to controls (Fig. 2c). The levels of arachidonic acid and bioactive lipid mediators generated from the cyclooxygenase and lipoxygenase pathways were significantly increased in kidney cortex of AKI donors compared to control (Fig. 2d, Supplementary Table 6). Integrated transcriptomic and metabolomic AKI-induced changes in arachidonic acid metabolism suggests that high levels of metabolites in the cyclooxygenase pathway (e.g. PGE2) and lipoxygenase pathway (e.g. 20-OH-LTB4) are generated in human kidneys following AKI (Fig. 2e).

Because arachidonic acid is generated from lipids, we investigated whether AKI impacts the abundance of serum and renal lipid species in humans. Liquid chromatography-mass spectrometry (LC-MS)-based lipidomic analysis was performed to investigate the levels of various lipid species in the serum and kidney samples, and the data was correlated with the eGFR of donors. A total of 423 serum lipid and 499 kidney lipid species were detected in human donors, and the levels of the top 50 lipids that were differentially expressed are presented as heatmap (Fig. 3a and c). In comparison to control, low levels of some lysophospholipids (mainly LPC and LPE) and phosphatidylinositol species were detected in the serum of donors with AKI (Fig. 3a). Pearson correlation analysis showed that, of the 423 lipid species detected in serum, 88 significantly correlated ($p<0.05$) with the eGFR (Supplementary Table 2). Interestingly, 6 lysophosphatidylcholine (LPC) species were the most positively correlated lipid species ($p<0.0001$), while linoleic acid (FFA_(18:2)), which is an important precursor of arachidonic acid, was the most negatively correlated serum lipid ($p=0.003$) with the eGFR of kidney donors (Fig 3b). Using sparse

partial-least square discriminant analysis (sPLS-DA), we showed that LPC_(14:0) is the most discriminant lipid species in the serum of donors with AKI donors compared to control (Supplementary Fig. 3b). This finding suggests that low levels of LPC_(14:0) may be a good serum lipid biomarker for human AKI.

Among the top 50 differentially abundant renal lipid species following AKI, decreased levels of several cardiolipins (CL), phosphatidylinositol (PI) and sphingomyelin (SM) species, and increased levels of several triglycerides (TG) and ceramide (Cer) species were detected in the kidney of donors with AKI (Fig. 3c). The decrease in renal PI and SM species were likely due to the low levels of these lipid species in the serum of donors with AKI (Supplementary Table 8 and 9). Interestingly, the renal accumulation of triglycerides and ceramide species in AKI kidneys were not linked to the levels of these lipid species in serum (Supplementary Table 8 and 9). Pearson correlation analysis showed that, of the 499 lipid species detected in the kidney, 104 significantly correlated ($p<0.05$) with the eGFR (Supplementary Table 3), with 8 lipid species shown to be the most significantly correlated ($p<0.0001$) (Fig. 3d, Supplementary Table 3). While three renal triglyceride and three ceramide species negatively correlated with the eGFR, two phosphatidylionositol species showed a positive correlation with the eGFR of human kidney donors (Fig. 3d). sPLS-DA analysis identified Cer_(36:1) as the most discriminant kidney lipid species (Supplementary Fig 3e) and volcano plot analysis showed that ceramide species make up 4 out of the 7 significantly impacted kidney lipid species following AKI (Supplementary Fig 3f). This finding is consistent with previous reports that acute renal tubular injury in mice and human proximal tubular (HK-2) cells causes ceramide accumulation [56,57]. There is evidence that ceramide-1-phosphate, a derivative of ceramide, increases cPLA2 activity [58] leading to enhanced mobilization of fatty acid from phospholipids, thus, promoting renal triglyceride synthesis and accumulation in HK-2 cells [59]. In keeping with these findings, and the evidence implicating cPLA2 in the pathophysiology of various forms of kidney disease [14-18], we hypothesize that AKI increases renal cPLA2-mediated phospholipid metabolism leading to the upregulation of arachidonic acid metabolism and the generation of pro-inflammatory eicosanoids (e.g. PGE2 and LTB4), thus, causing kidney damage in humans.

To test this hypothesis, the expression levels of the major enzymes involved in renal lipid metabolism in human kidneys following AKI were investigated. cPLA2 mRNA expression was significantly upregulated in the kidneys of donors with AKI compared to that of control donors (Fig. 3e), while CPT1A, CPT2, ACOX1, ACOX2, PPARA, PPARGC1A and CD36 expression levels were unchanged (Supplementary Fig. 4a-g). Western blots indicated that cPLA2 protein was significantly upregulated in human kidneys of donors with AKI (Fig. 3f), while CPT1A protein was unaffected (Supplementary Fig. 3h). Consistent with the upregulated cPLA2 levels, significantly higher levels of PGE2 were detected in the kidney tissue lysates of donors with AKI compared to control donors (Fig. 3g).

IMC Characterization of renal cortical immune cells following AKI

Based on evidence linking increased arachidonic acid metabolism to kidney inflammation [19], we used imaging mass cytometry to characterize the immune cell landscape of the kidneys collected from AKI donors and compared with control donors. Images of immune cell markers (Fig. 4 and Supplementary Fig

6), nestin, vimentin (Supplementary Fig. 7), CD31, α-SMA (Supplementary Fig. 8), collagen, pan cytokeratin (PanCK) (Supplementary Fig. 9), megalin and ECadherin (Supplementary Fig. 10), were acquired and analyzed. To visualize the immune cell landscape in the human kidney cortex, markers of innate (CD68, CD163, CD11c) and adaptive immune cells (CD3, CD4, CD8a and CD20) were investigated. The proportion of cells in the kidney cortex (glomerular and tubulo-interstitial regions) expressing the different immune cell markers were analyzed and compared between AKI and control donors. The proportion of CD68-positive, CD163-positive and CD68/CD163-positive cells (monocyte and macrophages) (Fig. 4a-d), CD3-positive (T-lymphocytes) (Fig. 4e, f), CD20-positive (B-lymphocytes) (Fig 4e, g) and CD4-positive (helper T-lymphocytes) (Fig. 4i, j) was significantly higher in the cortex of AKI donors compared to control. Although not significant, the proportion of CD8-positive (cytotoxic T-lymphocytes) (Fig. 4i, k) and CD11-positive cells (Fig. 4e, h) showed an increased trend in response to AKI. The significant upregulation in the population of a subset of immune cells in the kidney of donors with AKI is consistent with the findings from the GSEA analysis demonstrating that biological processes and pathways associated with the immune system are significantly upregulated following AKI (Supplementary Fig. 5). The visualization of immune cells using IMC showed that their population increased in the tubulointerstitial region rather than the glomeruli (Fig 4a, e, i), suggesting that damage to tubular epithelial cells may be driving inflammation in the injured kidney. Based on this finding, we speculate that the upregulated renal arachidonic acid pathway following AKI may be mediating inflammation in RPTECs

Validation of cPLA2-arachidonic acid pathway in mediating AKI

To investigate the role of cPLA2-arachidonic acid pathway in mediating inflammation in RPTECs following AKI, we carried out *in vitro* experiment using a cPLA2 inhibitor. RPTECs were either treated with cPLA2 inhibitor (10 or 100 μM) or vehicle. Since IL-1β was significantly higher in the kidneys of donors with AKI (Fig. 1k), we treated RPTECs with IL-1β to induce injury and the levels of PGE2, KIM-1, IL-6, IL-8 and TNF-α were measured in cell culture supernatant after 6 hours (Fig. 5a). IL-1β treatment significantly increased PGE2, KIM-1, IL-6, IL-8 and TNF-α levels in cell culture supernatant (Fig 5b-f). The supernatant collected from cells treated with 10 μM or 100 μM cPLA2 inhibitor + IL-1β had significantly lower levels of PGE2, KIM-1, IL-6 and IL-8, but not TNF-α, compared to cells treated with IL-1β only (Fig. 5b-f). Taken together, these findings demonstrate that the inhibition of cPLA2 ameliorates injury and inflammation in RPTECs in vitro. To test the efficacy of this inhibitor in freshly collected human kidney tissue, we used a human kidney organ culture model [51]. Cortical tissue fragments were obtained from 4 kidneys and treated with IL-1β, with or without 100 μM cPLA2 inhibitor, and cell culture supernatant were collected after 12 hours to investigate the levels of PGE2 and KIM-1 (Fig. 5g). The change in the levels of these markers were compared between IL-1β-treated tissue and cPLA2 inhibitor + IL-1β-treated tissue. The inhibition of cPLA2 significantly reduced PGE2 levels (Fig. 5h), while a trend for reduced KIM-1 levels (Fig. 5i) was seen in culture supernatant following IL-1β treatment. These findings demonstrate that inhibiting cPLA2 activity in human kidney cortex reduces PGE2 production and potentially ameliorates PGE2-mediated kidney injury *ex vivo*.

Discussion

The application of omics technologies and imaging mass cytometry to study the biology of the kidney has greatly improved our understanding of the molecular and cellular changes associated with kidney diseases. While these approaches accelerate our ability to perform in-depth analysis of the complex pathophysiology of AKI in humans and potentially aid the discovery of new therapies for this condition, the limited availability of kidney tissue from patients has remained a major challenge. To address this problem, we sought to establish whether kidney tissue from deceased organ transplant donors with or without pre-donation AKI could be utilized as a reliable experimental model to study human AKI at an unprecedented high-resolution. We show for the first time that kidneys from deceased transplant organ donors that had AKI during the last few days leading to organ donation retain the biological signature of this condition when compared with data from urine or kidney tissue of living patients [53,54,60]. The use of deceased human kidneys to study AKI benefits from the natural variation that exists in human samples and displays the heterogeneity that has been suggested to be incorporated in pre-clinical studies to improve therapeutic responses [61]. Moreover, the majority of patients with AKI are known to have severe underlying illness and comorbidities [62]. These factors are commonly associated with deceased donors, and a better understanding of the pathophysiology of human AKI using kidneys from these donors will aid the identification of therapeutic targets that are more likely to be clinically beneficial for patients.

The pathophysiology of human AKI varies according to the myriad of conditions associated with its development, however, oxidative stress associated with the dysregulation in kidney metabolism appears to be a consistent feature in the pathophysiology of all forms of AKI [63,64].

Because renal proximal tubular cells are the most energy consuming cells in the kidney, these cells are the most affected by the dysregulated kidney metabolism associated with AKI and are more prone to oxidative stress [65,66]. Importantly, cPLA2 has been reported to significantly contribute to the generation of reactive oxygen species and oxidative damage, which are associated with inflammation in proximal tubular cells following AKI [14,16,67]. In the current study, the consistently high levels of cPLA2 protein in human kidneys following AKI, and the reduced levels of KIM-1 and inflammatory cytokines associated with the inhibition of this enzyme in proximal tubular cells, suggest that this enzyme may be contributing to AKI-induced oxidative damage and kidney inflammation in humans. It is worth noting that while the IL-1β-induced increase in the levels of IL-6 and IL-8 were significantly reduced in RPTECs following cPLA2 inhibition, TNF-α levels were unchanged. It is possible that cPLA2 inhibition results in the amelioration of kidney inflammation via a pathway that is downstream of TNF- α. There is evidence that TNF-α induces the expression and activity of cPLA2, leading to an increase in the release of arachidonic acid and pro-inflammatory eicosanoids [68,69]. Therefore, the inhibition of the activity of cPLA2 is unlikely to have any impact on the levels of TNF-α. Based on these findings, we speculate that the inhibition of cPLA2 reduces the pro-inflammatory effect of TNF-α in human RPTECs, thus leading to the production of lower levels of IL-6 and IL-8 in response to AKI.

Although there is a paucity of information regarding the levels of cPLA2 protein in response to AKI in other renal cell types in humans, single cell transcriptomics data has shown that high levels of the cPLA2 gene are seen in mesangial cells and podocytes in the kidneys of patients with early diabetic nephropathy [70]. The inhibition of cPLA2 in mesangial cells suppresses inflammation by preventing the activation of the nuclear factor kappa B pathway in vitro [71], suggesting that cPLA2 may be mediating glomerular damage in humans following diabetes-induced kidney injury. In addition, high levels of the cPLA2 gene have been detected in renal macrophages and monocytes in the adult human kidney [72,73]. In the current study, we demonstrated that there are high levels of CD68-positive and CD163-positive macrophages in the kidney obtained from donors with AKI. Based on the findings that upregulated levels of cPLA2 protein is detected in the kidney of donors with AKI in the current study, it is possible that the levels of cPLA2 in renal macrophages, together with mesangial cells and podocytes, are upregulated following kidney injury in these donors. cPLA2-mediated release of pro-inflammatory eicosanoids from these cell types may be contributing to the renal inflammatory process following AKI. In support of this, there is evidence that phagocytic immune cells require cPLA2 to generate arachidonic acid and inflammatory eicosanoids in order to mediate inflammation [74-76]. For example, bone-marrow specific knockout of cPLA2 reduced renal macrophage infiltration, pro-inflammatory eicosanoids and cytokine (TNF-α and CCL2) levels following kidney injury induced by unilateral ureteral obstruction in mice [76]. Therefore, in addition to the findings in RPTECs, inhibiting cPLA2 in bone marrow-derived or circulating immune cells *in vivo* may be beneficial in ameliorating epithelial cell damage and kidney inflammation following AKI. Recent evidence suggests that another class of PLA2, lipoprotein-associated PLA2, mediates immunometabolic processes in humans and the inactivation of this protein protects against inflammation [77].

In summary, this is the first study to validate the use of kidneys from deceased transplant organ donors as a model of AKI. Because of the difficulty in obtaining human kidney biopsies from AKI patients, our validated human model of AKI offers an exceptional opportunity to study the complex mechanisms underpinning this condition. However, unlike kidney biopsies from living donors with AKI, a major limitation of this work is the impact of the relatively longer cold ischemia in kidney biopsies from deceased donors on the multi-omics landscape of AKI. Nevertheless, using this model, we show that arachidonic acid metabolism is significantly upregulated in human kidneys collected from deceased donors with AKI, a finding that is consistent with high levels of cPLA2 in these kidneys. The inhibition of this enzyme in human RPTECs reduces kidney injury and inflammation. Together, these findings suggest a key role for renal cPLA2-mediated arachidonic acid metabolism in mediating kidney inflammation following AKI in humans and warrants further investigation as a potential therapeutic target.

Declarations

Acknowledgments

We are grateful to the donors, donor families and National Health Service Blood transfusion and Transplantation (NHSBT) for access to human samples; Karolina Nilsson from Medicinal Chemistry department at AstraZeneca for providing the cPLA2 inhibitor; Julia Lindgren for coordinating the RNA-sequencing workflow. This work was funded from a research collaboration grant by AstraZeneca.

Author contribution

E.O.A., S.R., K.S.-P., and K.W. designed the study. E.O.A., M.M.H., J.Y.T., S.H., S.L., F.N.K., B.J., D.J., R.A. and B.M. performed the experiments and analyzed the data. E.O.A., K.S.-P., and K.W wrote the manuscript. All authors reviewed and edited the manuscript.

Disclosure/competing interests

E.O.A, B.M., J.Y.T., S.H., S.L., D.J., R.A., P.B.L.H. and K.W. are currently employed by AstraZeneca.

References

1 Gerhardt, L. M. S. & McMahon, A. P. Multi-omic approaches to acute kidney injury and repair. *Curr Opin Biomed Eng* **20**, doi:10.1016/j.cobme.2021.100344 (2021).

2 Chertow, G. M., Burdick, E., Honour, M., Bonventre, J. V. & Bates, D. W. Acute kidney injury, mortality, length of stay, and costs in hospitalized patients. *Journal of the American Society of Nephrology* **16**, 3365-3370, doi:10.1681/ASN.2004090740 (2005).

3 Chawla, L. S., Eggers, P. W., Star, R. A. & Kimmel, P. L. Acute kidney injury and chronic kidney disease as interconnected syndromes. *N Engl J Med* **371**, 58-66, doi:10.1056/NEJMra1214243 (2014).

4 Negi, S., Koreeda, D., Kobayashi, S., Iwashita, Y. & Shigematu, T. Renal replacement therapy for acute kidney injury. *Renal Replacement Therapy* **2**, 31, doi:10.1186/s41100-016-0043-1 (2016).

5 Zuk, A. *et al.* Overcoming Translational Barriers in Acute Kidney Injury: A Report from an NIDDK Workshop. *Clin J Am Soc Nephrol* **13**, 1113-1123, doi:10.2215/CJN.06820617 (2018).

6 Fiorentino, M. & Kellum, J. A. Improving Translation from Preclinical Studies to Clinical Trials in Acute Kidney Injury. *Nephron* **140**, 81-85, doi:10.1159/000489576 (2018).

7 Mestas, J. & Hughes, C. C. Of mice and not men: differences between mouse and human immunology. *J Immunol* **172**, 2731-2738, doi:10.4049/jimmunol.172.5.2731 (2004).

8 Park, J. G. *et al.* Immune cell composition in normal human kidneys. *Sci Rep* **10**, 15678, doi:10.1038/s41598-020-72821-x (2020).

9 Bonventre, J. V. & Zuk, A. Ischemic acute renal failure: an inflammatory disease? *Kidney Int* **66**, 480-485, doi:10.1111/j.1523-1755.2004.761_2.x (2004).

10 Simon, N. & Hertig, A. Alteration of Fatty Acid Oxidation in Tubular Epithelial Cells: From Acute Kidney Injury to Renal Fibrogenesis. *Front Med (Lausanne)* **2**, 52, doi:10.3389/fmed.2015.00052 (2015).

11 Herman-Edelstein, M., Scherzer, P., Tobar, A., Levi, M. & Gafter, U. Altered renal lipid metabolism and renal lipid accumulation in human diabetic nephropathy. *J Lipid Res* **55**, 561-572, doi:10.1194/jlr.P040501 (2014).

12 Li, S. *et al.* Transgenic expression of proximal tubule peroxisome proliferator-activated receptor-alpha in mice confers protection during acute kidney injury. *Kidney Int* **76**, 1049-1062, doi:10.1038/ki.2009.330 (2009).

13 Kang, H. M. *et al.* Defective fatty acid oxidation in renal tubular epithelial cells has a key role in kidney fibrosis development. *Nat Med* **21**, 37-46, doi:10.1038/nm.3762 (2015).

14 Al Asmari, A. K., Al Sadoon, K. T., Obaid, A. A., Yesunayagam, D. & Tariq, M. Protective effect of quinacrine against glycerol-induced acute kidney injury in rats. *BMC Nephrol* **18**, 41, doi:10.1186/s12882-017-0450-8 (2017).

15 Chang, J. F. *et al.* Targeting ROS and cPLA2/COX2 Expressions Ameliorated Renal Damage in Obese Mice with Endotoxemia. *Int J Mol Sci* **20**, doi:10.3390/ijms20184393 (2019).

16 Cui, X. L. *et al.* Oxidative signaling in renal epithelium: Critical role of cytosolic phospholipase A2 and p38(SAPK). *Free Radic Biol Med* **41**, 213-221, doi:10.1016/j.freeradbiomed.2006.02.004 (2006).

17 Khan, N. S. *et al.* Cytosolic Phospholipase A2alpha Is Essential for Renal Dysfunction and End-Organ Damage Associated With Angiotensin II-Induced Hypertension. *Am J Hypertens* **29**, 258-265, doi:10.1093/ajh/hpv083 (2016).

18 Bonventre, J. V. The 85-kD cytosolic phospholipase A2 knockout mouse: a new tool for physiology and cell biology. *J Am Soc Nephrol* **10**, 404-412, doi:10.1681/asn.V102404 (1999).

19 Wang, T. *et al.* Arachidonic Acid Metabolism and Kidney Inflammation. *Int J Mol Sci* **20**, doi:10.3390/ijms20153683 (2019).

20 Makino, H. *et al.* Prevention of diabetic nephropathy in rats by prostaglandin E receptor EP1-selective antagonist. *J Am Soc Nephrol* **13**, 1757-1765, doi:10.1097/01.asn.0000019782.37851.bf (2002).

21 Nasrallah, R., Xiong, H. & Hébert, R. L. Renal prostaglandin E2 receptor (EP) expression profile is altered in streptozotocin and B6-Ins2Akita type I diabetic mice. *Am J Physiol Renal Physiol* **292**, F278-284, doi:10.1152/ajprenal.00089.2006 (2007).

22 Ranganathan, P. V., Jayakumar, C., Mohamed, R., Dong, Z. & Ramesh, G. Netrin-1 regulates the inflammatory response of neutrophils and macrophages, and suppresses ischemic acute kidney injury by

inhibiting COX-2-mediated PGE2 production. *Kidney Int* **83**, 1087-1098, doi:10.1038/ki.2012.423 (2013).

23 Peters-Golden, M. & Henderson, W. R. Leukotrienes. *New England Journal of Medicine* **357**, 1841-1854, doi:10.1056/NEJMra071371 (2007).

24 Wei, Q., Xiao, X., Fogle, P. & Dong, Z. Changes in metabolic profiles during acute kidney injury and recovery following ischemia/reperfusion. *PLoS One* **9**, e106647, doi:10.1371/journal.pone.0106647 (2014).

25 Garcia-Pastor, C., Benito-Martinez, S., Bosch, R. J., Fernandez-Martinez, A. B. & Lucio-Cazana, F. J. Intracellular prostaglandin E2 contributes to hypoxia-induced proximal tubular cell death. *Sci Rep* **11**, 7047, doi:10.1038/s41598-021-86219-w (2021).

26 Brennan, E., Kantharidis, P., Cooper, M. E. & Godson, C. Pro-resolving lipid mediators: regulators of inflammation, metabolism and kidney function. *Nature Reviews Nephrology* **17**, 725-739, doi:10.1038/s41581-021-00454-y (2021).

27 Baek, J., He, C., Afshinnia, F., Michailidis, G. & Pennathur, S. Lipidomic approaches to dissect dysregulated lipid metabolism in kidney disease. *Nat Rev Nephrol* **18**, 38-55, doi:10.1038/s41581-021-00488-2 (2022).

28 Lin, P. H. & Duann, P. Dyslipidemia in Kidney Disorders: Perspectives on Mitochondria Homeostasis and Therapeutic Opportunities. *Front Physiol* **11**, 1050, doi:10.3389/fphys.2020.01050 (2020).

29 Muto, Y. *et al.* Single cell transcriptional and chromatin accessibility profiling redefine cellular heterogeneity in the adult human kidney. *Nature Communications* **12**, 2190, doi:10.1038/s41467-021-22368-w (2021).

30 Liao, J. *et al.* Single-cell RNA sequencing of human kidney. *Scientific Data* **7**, 4, doi:10.1038/s41597-019-0351-8 (2020).

31 Dannhorn, A. *et al.* Universal Sample Preparation Unlocking Multimodal Molecular Tissue Imaging. *Analytical Chemistry* **92**, 11080-11088, doi:10.1021/acs.analchem.0c00826 (2020).

32 Swales, J. G. *et al.* Quantitation of Endogenous Metabolites in Mouse Tumors Using Mass-Spectrometry Imaging. *Anal Chem* **90**, 6051-6058, doi:10.1021/acs.analchem.7b05239 (2018).

33 Dannhorn, A. *et al.* Evaluation of UV-C Decontamination of Clinical Tissue Sections for Spatially Resolved Analysis by Mass Spectrometry Imaging (MSI). *Anal Chem* **93**, 2767-2775, doi:10.1021/acs.analchem.0c03430 (2021).

34 Takáts, Z., Wiseman, J. M., Gologan, B. & Cooks, R. G. Mass spectrometry sampling under ambient conditions with desorption electrospray ionization. *Science* **306**, 471-473,

doi:10.1126/science.1104404 (2004).

35 Adusumilli, R. & Mallick, P. Data Conversion with ProteoWizard msConvert. *Methods Mol Biol* **1550**, 339-368, doi:10.1007/978-1-4939-6747-6_23 (2017).

36 Race, A. M., Styles, I. B. & Bunch, J. Inclusive sharing of mass spectrometry imaging data requires a converter for all. *J Proteomics* **75**, 5111-5112, doi:10.1016/j.jprot.2012.05.035 (2012).

37 Pang, Z. *et al.* MetaboAnalyst 5.0: narrowing the gap between raw spectra and functional insights. *Nucleic Acids Res* **49**, W388-W396, doi:10.1093/nar/gkab382 (2021).

38 Kanehisa, M. *et al.* Data, information, knowledge and principle: back to metabolism in KEGG. *Nucleic Acids Res* **42**, D199-205, doi:10.1093/nar/gkt1076 (2014).

39 Okonechnikov, K., Conesa, A. & García-Alcalde, F. Qualimap 2: advanced multi-sample quality control for high-throughput sequencing data. *Bioinformatics (Oxford, England)* **32**, 292-294, doi:10.1093/bioinformatics/btv566 (2016).

40 Dobin, A. *et al.* STAR: ultrafast universal RNA-seq aligner. *Bioinformatics* **29**, 15-21, doi:10.1093/bioinformatics/bts635 (2013).

41 Ewels, P., Magnusson, M., Lundin, S. & Käller, M. MultiQC: summarize analysis results for multiple tools and samples in a single report. *Bioinformatics* **32**, 3047-3048, doi:10.1093/bioinformatics/btw354 (2016).

42 Gaspar, J. M. NGmerge: merging paired-end reads via novel empirically-derived models of sequencing errors. *BMC Bioinformatics* **19**, 536, doi:10.1186/s12859-018-2579-2 (2018).

43 Patro, R., Duggal, G., Love, M. I., Irizarry, R. A. & Kingsford, C. Salmon provides fast and bias-aware quantification of transcript expression. *Nat Methods* **14**, 417-419, doi:10.1038/nmeth.4197 (2017).

44 Ashburner, M. *et al.* Gene Ontology: tool for the unification of biology. *Nature Genetics* **25**, 25-29, doi:10.1038/75556 (2000).

45 Yu, G., Wang, L. G., Han, Y. & He, Q. Y. clusterProfiler: an R package for comparing biological themes among gene clusters. *OMICS* **16**, 284-287, doi:10.1089/omi.2011.0118 (2012).

46 Luo, W. & Brouwer, C. Pathview: an R/Bioconductor package for pathway-based data integration and visualization. *Bioinformatics* **29**, 1830-1831, doi:10.1093/bioinformatics/btt285 (2013).

47 Jenkins, B., Ronis, M. & Koulman, A. LC–MS Lipidomics: Exploiting a Simple High-Throughput Method for the Comprehensive Extraction of Lipids in a Ruminant Fat Dose-Response Study. *Metabolites* **10**, 296 (2020).

48 Elaldi, R. *et al.* High Dimensional Imaging Mass Cytometry Panel to Visualize the Tumor Immune Microenvironment Contexture. *Front Immunol* **12**, 666233, doi:10.3389/fimmu.2021.666233 (2021).

49 Bass, J. J. *et al.* An overview of technical considerations for Western blotting applications to physiological research. *Scand J Med Sci Sports* **27**, 4-25, doi:10.1111/sms.12702 (2017).

50 Al-Lamki, R. S. *et al.* Tumor necrosis factor receptor expression and signaling in renal cell carcinoma. *Am J Pathol* **177**, 943-954, doi:10.2353/ajpath.2010.091218 (2010).

51 Al-Lamki, R. S., Bradley, J. R. & Pober, J. S. Human Organ Culture: Updating the Approach to Bridge the Gap from In Vitro to In Vivo in Inflammation, Cancer, and Stem Cell Biology. *Front Med (Lausanne)* **4**, 148, doi:10.3389/fmed.2017.00148 (2017).

52 Sparrow, H. G., Swan, J. T., Moore, L. W., Gaber, A. O. & Suki, W. N. Disparate outcomes observed within Kidney Disease: Improving Global Outcomes (KDIGO) acute kidney injury stage 1. *Kidney Int* **95**, 905-913, doi:10.1016/j.kint.2018.11.030 (2019).

53 Han, W. K., Bailly, V., Abichandani, R., Thadhani, R. & Bonventre, J. V. Kidney Injury Molecule-1 (KIM-1): A novel biomarker for human renal proximal tubule injury. *Kidney International* **62**, 237-244, doi:https://doi.org/10.1046/j.1523-1755.2002.00433.x (2002).

54 Alge, J. L. & Arthur, J. M. Biomarkers of AKI: a review of mechanistic relevance and potential therapeutic implications. *Clin J Am Soc Nephrol* **10**, 147-155, doi:10.2215/CJN.12191213 (2015).

55 Kurzhagen, J. T., Dellepiane, S., Cantaluppi, V. & Rabb, H. AKI: an increasingly recognized risk factor for CKD development and progression. *J Nephrol* **33**, 1171-1187, doi:10.1007/s40620-020-00793-2 (2020).

56 Kalhorn, T. & Zager, R. A. Renal cortical ceramide patterns during ischemic and toxic injury: assessments by HPLC-mass spectrometry. *Am J Physiol* **277**, F723-733, doi:10.1152/ajprenal.1999.277.5.F723 (1999).

57 Zager, R. A., Conrad, D. S. & Burkhart, K. Ceramide accumulation during oxidant renal tubular injury: mechanisms and potential consequences. *J Am Soc Nephrol* **9**, 1670-1680, doi:10.1681/asn.V991670 (1998).

58 Stahelin, R. V., Subramanian, P., Vora, M., Cho, W. & Chalfant, C. E. Ceramide-1-phosphate Binds Group IVA Cytosolic Phospholipase a2 via a Novel Site in the C2 Domain*. *Journal of Biological Chemistry* **282**, 20467-20474, doi:https://doi.org/10.1074/jbc.M701396200 (2007).

59 Zager, R. A., Johnson, A. C. & Hanson, S. Y. Renal tubular triglyercide accumulation following endotoxic, toxic, and ischemic injury. *Kidney Int* **67**, 111-121, doi:10.1111/j.1523-1755.2005.00061.x (2005).

60 Mishra, J. *et al.* Neutrophil gelatinase-associated lipocalin (NGAL) as a biomarker for acute renal injury after cardiac surgery. *Lancet* **365**, 1231-1238, doi:10.1016/s0140-6736(05)74811-x (2005).

61 de Caestecker, M. *et al.* Bridging Translation by Improving Preclinical Study Design in AKI. *J Am Soc Nephrol* **26**, 2905-2916, doi:10.1681/ASN.2015070832 (2015).

62 Girling, B. J., Channon, S. W., Haines, R. W. & Prowle, J. R. Acute kidney injury and adverse outcomes of critical illness: correlation or causation? *Clin Kidney J* **13**, 133-141, doi:10.1093/ckj/sfz158 (2020).

63 Ronco, C., Bellomo, R. & Kellum, J. A. Acute kidney injury. *The Lancet* **394**, 1949-1964, doi:10.1016/s0140-6736(19)32563-2 (2019).

64 Nath, K. A. & Norby, S. M. Reactive oxygen species and acute renal failure. *The American Journal of Medicine* **109**, 665-678, doi:https://doi.org/10.1016/S0002-9343(00)00612-4 (2000).

65 Bhargava, P. & Schnellmann, R. G. Mitochondrial energetics in the kidney. *Nature Reviews Nephrology* **13**, 629-646, doi:10.1038/nrneph.2017.107 (2017).

66 Faivre, A., Verissimo, T., Auwerx, H., Legouis, D. & de Seigneux, S. Tubular Cell Glucose Metabolism Shift During Acute and Chronic Injuries. *Frontiers in Medicine* **8**, doi:10.3389/fmed.2021.742072 (2021).

67 Rehan, A., Johnson, K. J., Wiggins, R. C., Kunkel, R. G. & Ward, P. A. Evidence for the role of oxygen radicals in acute nephrotoxic nephritis. *Lab Invest* **51**, 396-403 (1984).

68 Hoeck, W. G., Ramesha, C. S., Chang, D. J., Fan, N. & Heller, R. A. Cytoplasmic phospholipase A2 activity and gene expression are stimulated by tumor necrosis factor: dexamethasone blocks the induced synthesis. *Proceedings of the National Academy of Sciences* **90**, 4475-4479, doi:10.1073/pnas.90.10.4475 (1993).

69 Yang, C. M. *et al.* TNF-alpha induces cytosolic phospholipase A2 expression via Jak2/PDGFR-dependent Elk-1/p300 activation in human lung epithelial cells. *Am J Physiol Lung Cell Mol Physiol* **306**, L543-551, doi:10.1152/ajplung.00320.2013 (2014).

70 Wilson, P. C. *et al.* The single-cell transcriptomic landscape of early human diabetic nephropathy. *Proc Natl Acad Sci U S A* **116**, 19619-19625, doi:10.1073/pnas.1908706116 (2019).

71 Huwiler, A. *et al.* The ω3-polyunsaturated fatty acid derivatives AVX001 and AVX002 directly inhibit cytosolic phospholipase A2and suppress PGE2formation in mesangial cells. *British Journal of Pharmacology* **167**, 1691-1701, doi:10.1111/j.1476-5381.2012.02114.x (2012).

72 Wu, H. *et al.* Single-Cell Transcriptomics of a Human Kidney Allograft Biopsy Specimen Defines a Diverse Inflammatory Response. *Journal of the American Society of Nephrology : JASN* **29**, 2069-2080,

doi:10.1681/ASN.2018020125 (2018).

73 Menon, R. *et al.* Single cell transcriptomics identifies focal segmental glomerulosclerosis remission endothelial biomarker. *JCI Insight* **5**, doi:10.1172/jci.insight.133267 (2020).

74 Dabral, D. & van den Bogaart, G. The Roles of Phospholipase A2 in Phagocytes. *Front Cell Dev Biol* **9**, 673502, doi:10.3389/fcell.2021.673502 (2021).

75 Gijón, M. A., Spencer, D. M., Siddiqi, A. R., Bonventre, J. V. & Leslie, C. C. Cytosolic phospholipase A2 is required for macrophage arachidonic acid release by agonists that Do and Do not mobilize calcium. Novel role of mitogen-activated protein kinase pathways in cytosolic phospholipase A2 regulation. *J Biol Chem* **275**, 20146-20156, doi:10.1074/jbc.M908941199 (2000).

76 Montford, J. R. *et al.* Bone marrow-derived cPLA2alpha contributes to renal fibrosis progression. *J Lipid Res* **59**, 380-390, doi:10.1194/jlr.M082362 (2018).

77 Spadaro, O. *et al.* Caloric restriction in humans reveals immunometabolic regulators of health span. *Science* **375**, 671-677, doi:10.1126/science.abg7292 (2022).

Table

Table 1 is available in the Supplementary Files section

Figures

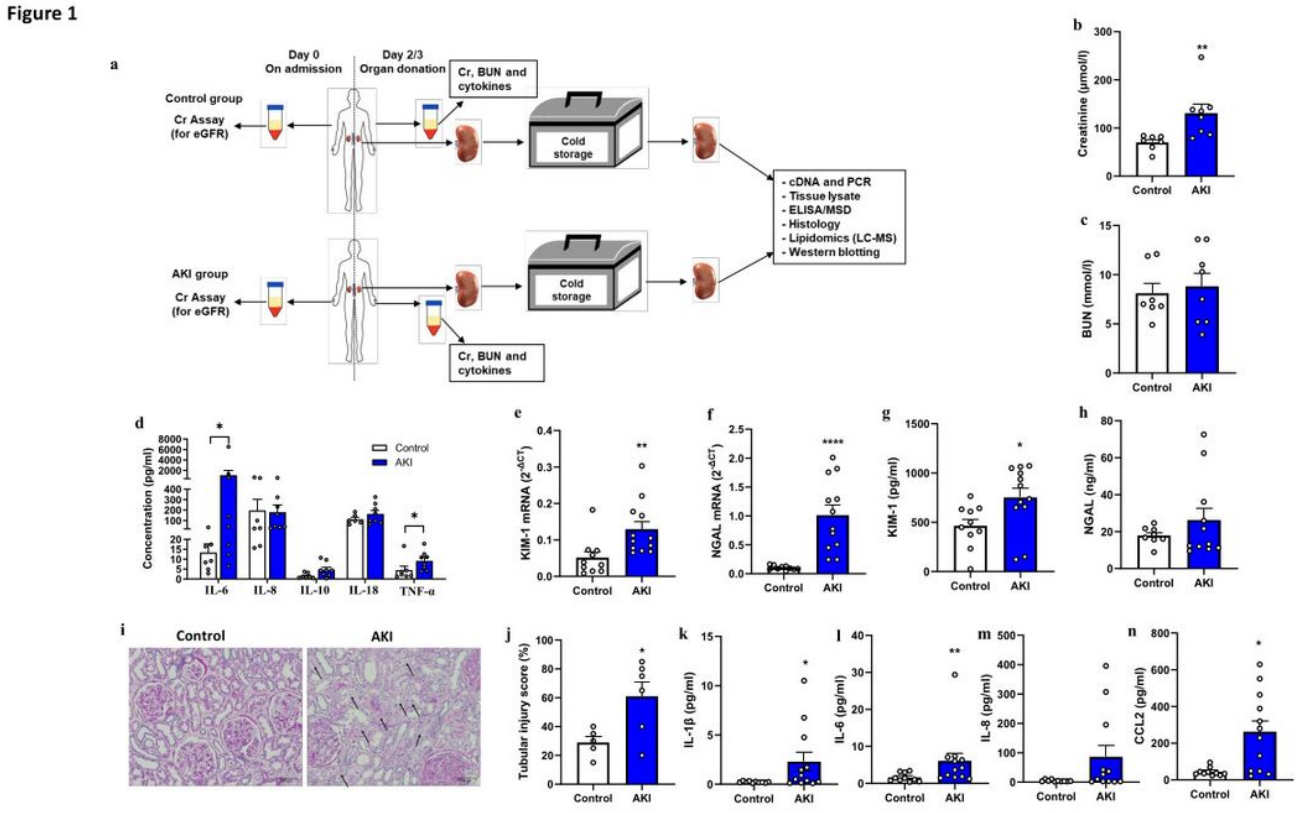

Figure 1

Kidney injury and inflammatory markers in human kidney donors (a) Schematic illustration of the experimental workflow from the point of admission of transplant organ donors into clinic to the point of kidney tissue collection in the laboratory. (b) Creatinine and (c) BUN in serum of kidney donors (n=7-8 donors). (d) Serum cytokine levels in control and AKI donors (n=6-8 donors). mRNA transcript levels of KIM-1 (e) and NGAL (f) in human kidneys (n=10-12 kidneys). Protein levels of KIM-1 (g) and NGAL (h) in kidney tissue lysate (n=8-12 kidneys). (i) PAS staining showing the morphology of the kidneys in both groups, with arrows indicating tubules with casts, damaged brush border membrane and vacuolization and (j) Tubular injury score expressed in percentage, with 0 % indicating no injury and 100 % indicating maximal injury in both groups of kidneys (n=5-6 kidneys). Protein levels of inflammatory markers in kidney tissue lysate: IL-1β (k), IL-6 (l), IL-8 (m) and CCL2 (n). Data is presented as mean ± SEM and statistical analysis was performed using a two-tailed Mann Whitney *U* test **P*<0.05, ***P*<0.01 and *****P*<0.0001.

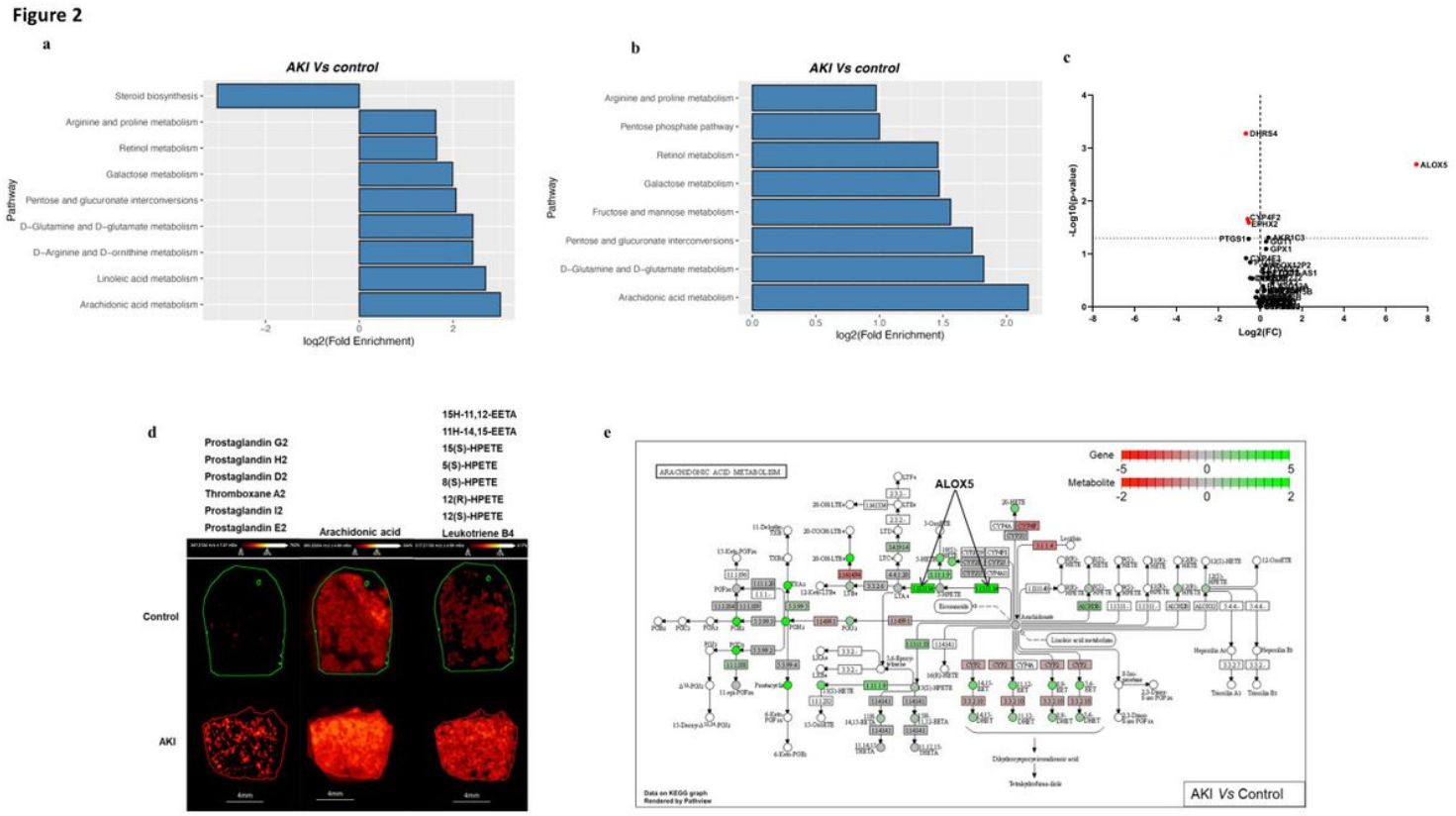

Figure 2

Integrated kidney metabolomics and transcriptomics. Pathway enrichment analysis showing significantly enriched pathways ($p<0.05$) using (a) untargeted metabolomics data and (b) integrated metabolomic and transcriptomic data in the kidney cortex following AKI. (c) Volcano plot showing $-\log_{10}$ of *P* value plotted against the $\log_2$ of fold change in the levels of genes involved in arachidonic acid metabolism, with the red dots representing lipids that are significantly altered in donors with AKI ($p<0.05$). (d) Representative mass-spectrometry images showing the changes in ionization levels of arachidonic acid and metabolites in the arachidonic acid pathway (e) KEGG pathway map depicting fold changes in gene expression and metabolites involved in arachidonic acid metabolism following AKI.

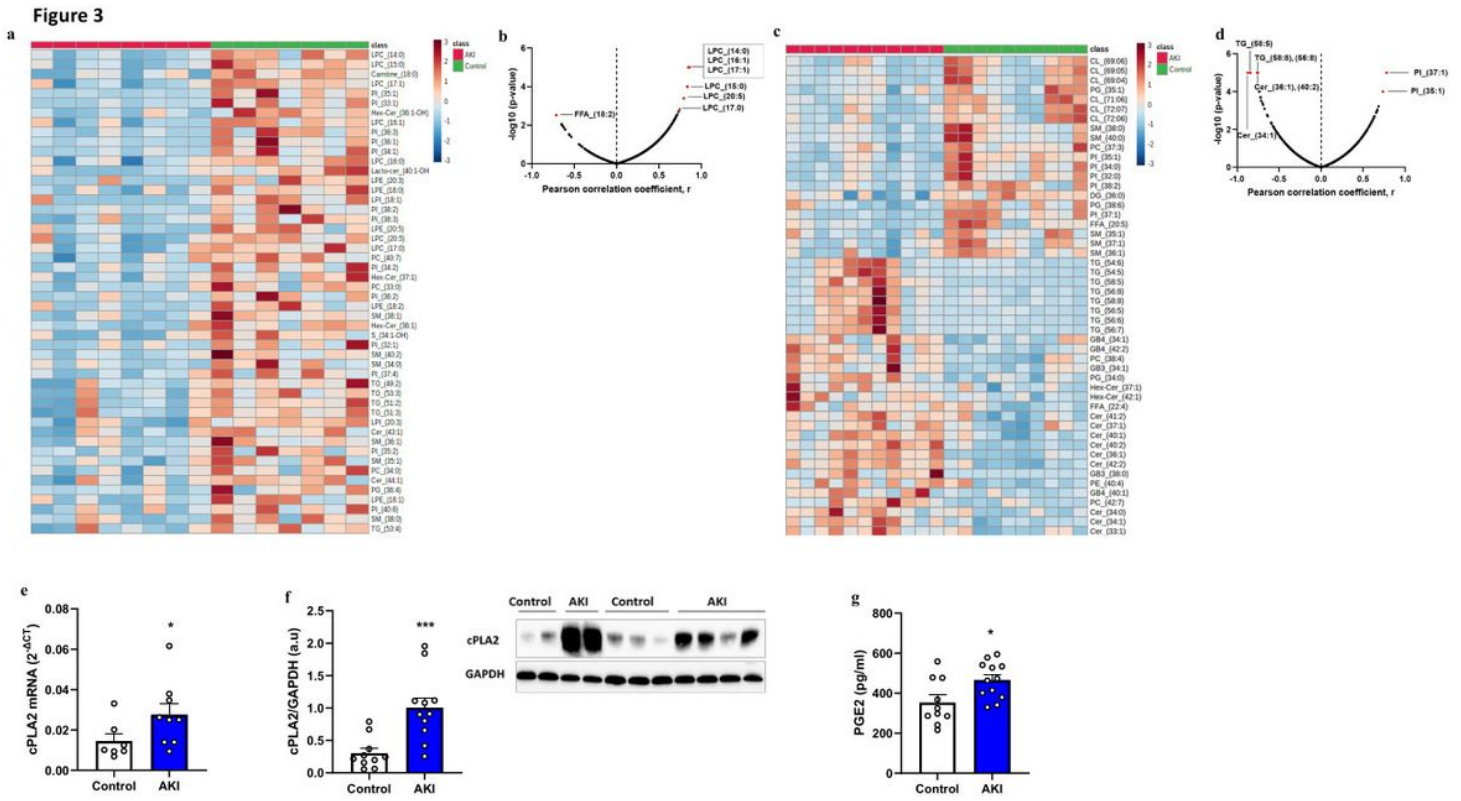

Figure 3

Changes in kidney lipid metabolism following AKI (a) Heatmap analysis showing the top 50 differentially expressed lipid species in serum of AKI and control donors (n=7-8 donors). (b) Volcano plot showing the -log10 of p-value and the Pearson correlation coefficient (r) obtained from the correlation analysis of the levels of serum lipid species with the eGFR of human kidney donors. Lipid species highlighted by red dots were the most significantly correlated with the eGRF of kidney donors. (c) Heatmap analysis showing the top 50 differentially expressed lipid species in the kidney cortex of AKI and control donors (n=10-11 kidneys). (d) Volcano plot showing the -log10 of p-value and the Pearson correlation coefficient (r) obtained from the correlation analysis of the levels of kidney lipid species with the eGFR of human kidney donors. Lipid species highlighted by red dots were the most significantly correlated with the eGRF of kidney donors. (e) Relative mRNA transcript levels of cPLA2 in kidney cortex of donors. PCR experiments were carried out using human specific cPLA2 primer and the mRNA transcript levels were expressed relative to the levels of HPRT1 (n=7-9 kidneys). (f) Western blotting showing the levels of cPLA2 protein, with representative images showing the band density of the protein (n=10-12 kidneys). The levels of PLA2 protein were expressed relative to GAPDH and presented in arbitrary units (a.u). (g) Renal tissue PGE2 levels investigated by ELISA (n=10-12). Data is presented as mean ± SEM and statistical analysis was performed using a two-tailed Mann Whitney *U* test, **P*<0.05 and ****P*<0.001

Figure 4

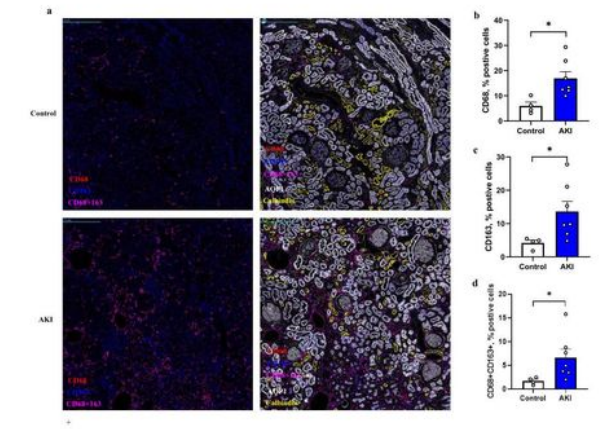

Figure 4

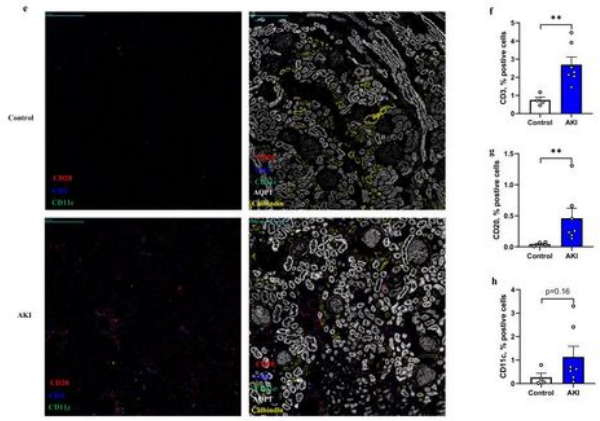

Figure 4

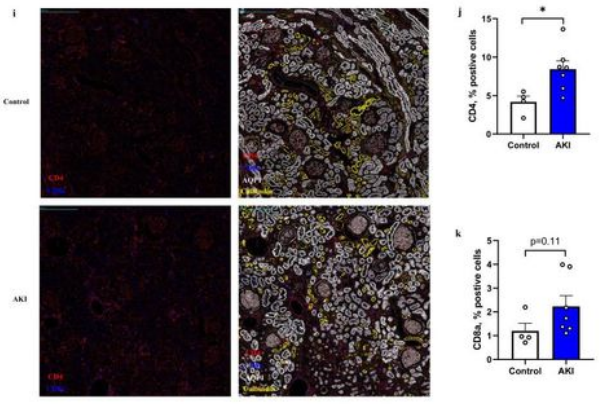

Figure 4

Characterization of renal immune cell landscape following AKI. (a) IMC image showing renal CD68 and CD163 expressing cells as indicated. Graphs showing proportion of (b) CD68-expressing cells, (c) CD163 expressing cells, (d) cells expressing both CD68 and CD163. (e) IMC image showing renal CD3, CD20 and CD11c expressing cells as indicated. Graphs showing proportion of (f) CD3 expressing cells, (g) CD20 expressing cells and (h) CD11c expressing cells. (i) IMC image showing renal CD4 and CD8a expressing

cells as indicated. Graphs showing proportion of (j) CD4 expressing cells, (k) CD8a-expressing cells. Aquaporin 1 (AQP1) and calbindin D28k was used to highlight the proximal tubular and distal tubular segments of the nephron (a, e, i) and scale bar: 360 µm. Data is presented as mean ± SEM and statistical analysis was performed using a two-tailed Mann Whitney *U* test **P*<0.05, ***P*<0.01.

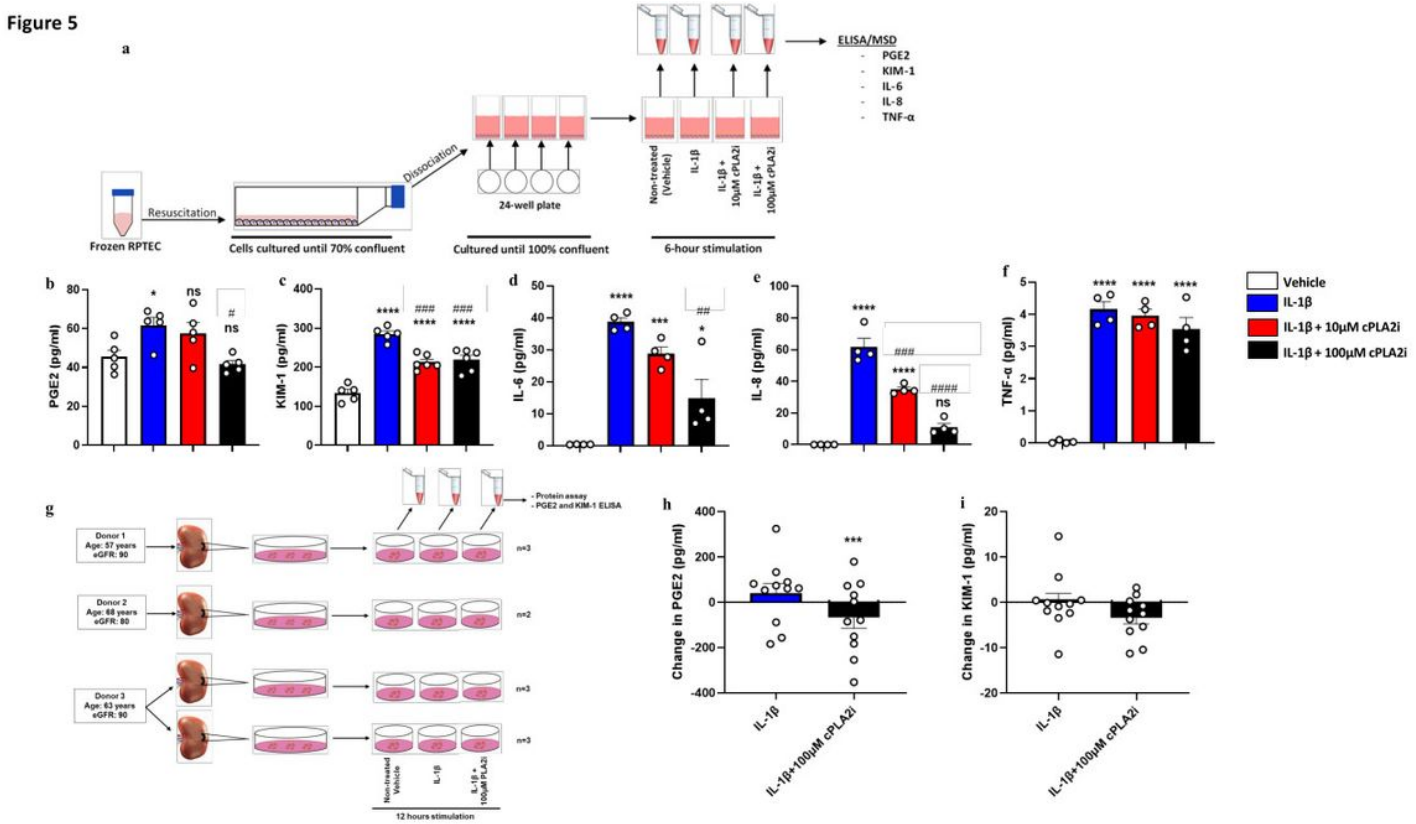

Figure 5

Inhibition of renal cPLA2 ameliorates kidney injury in vitro. (a) Schematic illustrating the experimental design of the in vitro experiment to test the impact of cPLA2 inhibition on kidney injury and inflammation. RPTECs were stimulated for 6 hours using IL-1β with or without cPLA2 inhibitor (cPLA2i), and culture supernatant were analyzed for the levels of: (b) PGE2 (c) KIM-1 (d) IL-6, (e) IL-8 (f) TNF-α (n=4-6). Statistical analysis was performed using a one-way ANOVA with Tukey's multiple comparison's tests to compare the vehicle and other groups, ns-not significant, **P*<0.05, ****P*<0.001, *****P*<0.0001; and to compare IL-1β and IL-1β + cPLA2i, $^{\#}P$<0.05, $^{\#\#}P$<0.01, $^{\#\#\#}P$<0.001, $^{\#\#\#\#}P$<0.0001. (g) Schematic illustration of human kidney organ culture experimental design to test the impact of cPLA2 inhibition on PGE2 and KIM-1 levels. Kidney tissue fragments were stimulated for 12 hours using IL-1β with or without cPLA2 inhibitor (cPLA2i), and culture supernatant were analyzed for the levels of PGE2 and KIM-1. The levels of these markers were normalized using the protein concentration of tissue culture supernatant obtained from each well. Change in the normalized levels of PGE2 and KIM-1 was determined by

subtracting the levels of these markers in untreated tissue supernatant from that of IL-1β-treated or IL-1β + cPLA2i treated tissue (n=11). A pair-wise comparison was performed using t-test, ***P<0.001.

Supplementary Files

This is a list of supplementary files associated with this preprint. Click to download.

- Table1.pdf
- ST1.pdf
- SupplementaryTable2.xlsx
- SupplementaryTable3.xlsx
- ST4.pdf
- ST5.pdf
- SupplementaryTable6kidneymetabolomicsFC.xlsx
- SupplementaryTable7kidneytranscriptomics.xlsx
- SupplementaryTable8serumlipidomics.xlsx
- SupplementaryTable9kidneylipidomics.xlsx